ADVANCED FUNCTIONAL MATERIALS
www.afm-journal.de

Engineering of Complex Macroporous Materials Through Controlled Electrodeposition in Colloidal Superstructures

Matthias Heim, Stéphane Reculusa, Serge Ravaine, and Alexander Kuhn**

Macroporous materials with a sophisticated architecture are obtained by electrochemical deposition of gold or polypyrrole in colloidal-crystal templates. The Langmuir–Blodgett technique enables assembly of sub-micrometric silica-particle monolayers on conductive gold substrates, thus leading to colloidal superstructures with an unprecedented control of their features at the single-bead-layer level. This allows the integration of deliberate planar defects or the elaboration of well-defined gradients in terms of sphere size. Controlled infiltration using electrochemical deposition preserves the architecture of the original templates and leads to inverse opals with well-defined pore structures after the removal of the inorganic particles.

1. Introduction

The creation of highly ordered macroporous materials has attracted great interest in the last few years due to a large number of applications in different domains, including electroanalysis,[1,2] photonic crystals,[3] actuators,[4] filters[5] and energy-storage or conversion devices.[6] In particular, macroporous structures provide higher surface areas than their flat homologues, which, combined with more-efficient mass transport in their sub-micrometer-sized pores, makes them very-interesting candidates for use as electrodes in biosensors[7] or biofuel cells.[8] Artificial opals and their inverse counterparts, used as filter membranes, have also enabled size-dependent separation of biomolecules (such as DNA or proteins) or colloidal particles, with the possibility of adapting the pore dimensions to a required separation profile.[5,9,10] The photonic properties of colloidal crystals and/or their replicas have also been studied as optical sensors for the detection of different solvents, heavy-metal ions and biomolecules.[11] One of the most-promising strategies for achieving photonic crystals, that exhibit a complete band gap in the UV–vis spectral region, is the infiltration of a 3D-colloidal crystal template with a high-refractive-index material.[12]

M. Heim, Prof. A. Kuhn
Université de Bordeaux
Institut des Sciences Moléculaires – CNRS UMR5255
ENSCBP, 16 Avenue Pey Berland, 33607 Pessac, France
E-mail: kuhn@enscbp.fr
Dr. S. Reculusa, Prof. S. Ravaine
Université de Bordeaux
Centre de Recherche Paul Pascal – CNRS, UPR8641
Avenue Albert Schweitzer, 33600 Pessac, France
E-mail: ravaine@crpp-bordeaux.cnrs.fr

DOI: 10.1002/adfm.201101918

Several techniques have been reported in the literature, describing the assembly of colloidal particles into organized structures, including gravity sedimentation,[13] electrophoretic assembly,[14] spin- or dip-coating,[15,16] convective self-assembly[17] and physical confinement.[18] Besides the fabrication of homogeneous colloidal crystals based on one single bead size, they also allow various superstructures to be built up, combining spheres of different size[19] or chemical composition[20] in one template. Additionally, point,[21,22] line[23] or planar[24–26] defects have been successfully integrated in colloidal crystals in order to explore their influence on the photonic properties of the material. A drawback of these assembly techniques, however, consists of the poor control over the number of particle layers deposited during the assembly process, hence leading to restrictions, for example when gradients in colloidal crystals with different sphere sizes in successive layers have to be produced. The few attempts made to fabricate graded colloidal-crystal structures have consisted of top-down modifications of previously assembled polystyrene spheres by heating[27] or plasma etching,[28] associated with a considerable lack of control over the resulting bead size and structure of the gradient. Such a limitation can, however, be overcome using a step-by-step assembly process of the colloidal basic units. In particular, successive transfers onto a solid substrate of a monolayer of surface-modified silica particles through the Langmuir–Blodgett (LB) technique has proved to result in colloidal-crystal assemblies with a thickness defined at the single-layer level.[29–31] Since Langmuir films can be prepared from silica particles with a range of different diameters,[32] architectures based on two different sizes have already been realized in the past using this approach.[33–36] In the current work, we have taken full advantage of the benefits of the LB process to build up colloidal superstructures with an unprecedented degree of complexity using up to six different particle sizes, the sequential deposition of monolayers allowing a predefined architecture to be generated exactly.

A second challenge consisted of getting the inverse replicas of these highly organized structures. As described by Velev and coworkers, strategies to get polymeric, metallic, semiconducting or inorganic porous materials starting from colloidal templates are quite numerous, such as UV-induced polymerization, chemical vapor deposition, particle infusion or sol-gel hydrolysis.[37,38] Among them, electrochemical deposition has been found to be one of the most convenient, since the

© 2012 WILEY-VCH Verlag GmbH & Co. KGaA, Weinheim

thickness of the inverse material (metal or conductive polymer) can be controlled quite precisely through the measurement of the global charge passed during the experiment.[39–41] Here, we have made the most out of recent contributions, where we demonstrated that chronoamperometric curves allow an even-more-direct control over the inverse material thickness when LB films deposited onto conductive substrates are used as templates.[6,7] Potentiostatic electrodepositions were therefore performed to infiltrate the colloidal superstructures synthesized previously. Despite the complexity of their architectures, the void spaces of these templates, regular and crack-free enough over large areas, were successfully filled with either gold or polypyrrole, with a constant control over the growth process. After removal of the silica matrix, the resulting materials were characterized by scanning electron microscopy (SEM). At the end of the multistep process, which is schematically represented in **Figure 1**, easily handleable macroporous structures with a well-defined and original architecture were finally obtained.

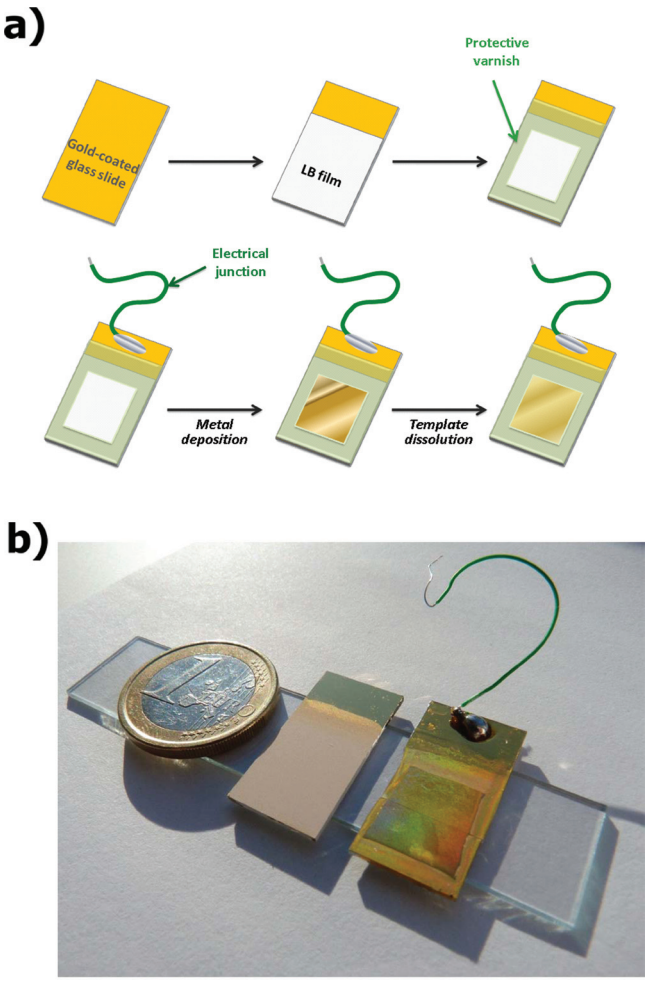

Figure 1. a) Representation of the different consecutive steps for the preparation of macroporous metallic materials. b) Picture of a gold-coated glass slide after the deposition of the colloidal template (middle) and at the end of the whole process (right).

2. Results and Discussion

2.1. Elaboration of the Colloidal Templates with the LB Technique

Amongst others, one of the great advantages of the LB technique is the possibility of building up colloidal crystals with control at the single-bead-layer level. As described in the Experimental Section, well-compressed monolayers of silica particles can be transferred from the air-water interface onto solid substrates and this process is repeated until the desired number of layers, up to several tens of layers, has been deposited on the sample. In this work, colloidal superstructures with various architectures using silica particles of different diameters were synthesized following this strategy. More precisely, three main families of templates with increasing complexity that may lead to various types of applications were generated: (Type-I) templates using two sizes of particles with a well-defined planar defect; (Type-II) templates using three sizes of particles assembled in a "single-gradient" structure; and, finally, (Type-III) "double-gradient" structures using particles of different sizes organized symmetrically with respect to a central layer consisting of the largest or smallest particles. It is worth noting that all of the colloidal-crystal templates fabricated were uniform over an area of more than 2 cm^2, as pictured in Figure 1b, but Langmuir–Blodgett films can be deposited perfectly well onto larger surfaces without any restrictions, as long as the required equipment, a Langmuir trough with a large working area and a sufficient immersion depth, is available.

As pictured in **Figure 2**, where SEM side views of all types of the samples are presented, the thicknesses and compositions of the templates are very regular. In particular, with the "Type-II" templates based on successive stacks of layers with increasing diameters of silica particles, the eventual irregularities of the first stackings had little influence on the arrangements of the upper ones, as shown in Figure 2b. It was, however, possible to take advantage of the specific iterative process, typical of the LB strategy, to get templates with an even-higher degree of complexity. Indeed, sequential stacking of single layers of particles with different diameters could lead to templates with a "double-gradient" (Type-III). Here, we focused on symmetrical architectures where the middle bead monolayer acted as a symmetry plane for the whole structure. In such cases, it makes a difference whether the bigger beads are positioned onto smaller ones or the other way round. In the latter sequence, care had to be taken to choose bead diameters that were not too different from one bead layer to the next, because otherwise the smaller beads would slide into the free space existing between the bigger beads, leading finally to ondulating layers (see upper layers in Figure 2c).

The template pictured in Figure 2c was assembled from 11 layers comprising beads of six different diameters ranging from 240 to 1200 nm. In this case, the particle diameter was gradually increased for the first six layers and decreased for the following five ones, leading to an "ascending-descending" architecture. By taking a close look at the template structure (see inset in Figure 2c), one can notice that the first six layers were homogeneously organized throughout the colloidal crystal, without any

© 2012 WILEY-VCH Verlag GmbH & Co. KGaA, Weinheim

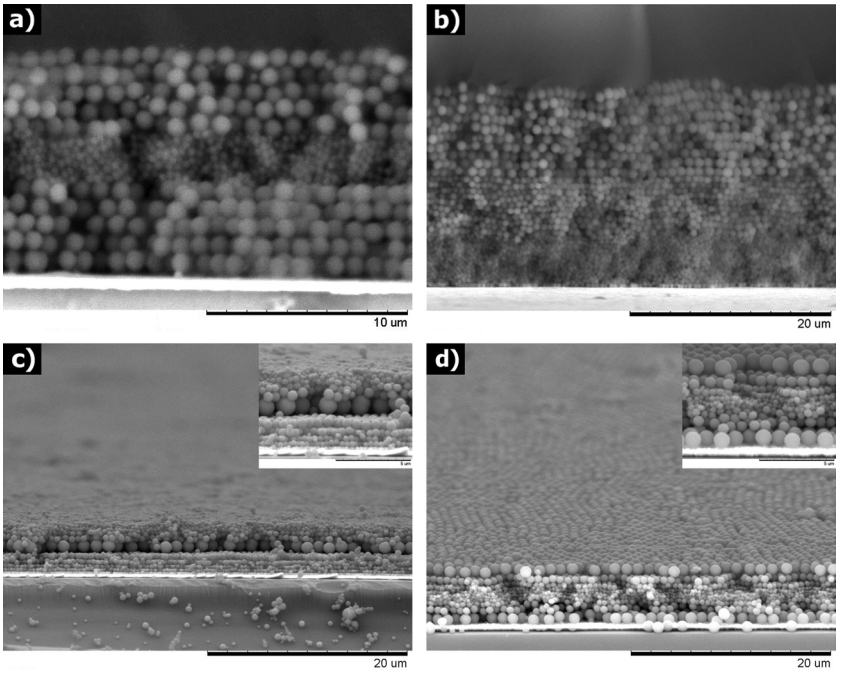

Figure 2. SEM side views of colloidal templates formed by Langmuir–Blodgett deposition of monolayers of silica particles on a gold-coated glass substrate. a) "Type-I" template with a 5-layer stack of 430 nm particles separating two 5-layer stacks of 1000 nm particles. b) "Type-II" monogradient template consisting of three 10-layer stacks of 430, 740 and 1000 nm particles. c–d) "Type-III" colloidal templates presenting a double-gradient structure consisting of consecutive monolayers of silica particles with different diameters: ascending-descending architecture with larger particles in the middle (240, 325, 395, 470, 600, 1200, 600, 470, 395, 325 and 240) (c); descending-ascending architecture with smaller particles in the middle (1000, 740, 470, 325, 240, 325, 470, 740 and 1000) (d).

significant variation in thickness. The remaining five layers, however, show a slightly wavy character, which was attributed to the fact that layers of smaller particle size were deposited onto bigger ones. It was possible to minimize this effect by selecting particles whose diameters varied only slightly from one layer to the next. In Figure 2d, a reverse type of template (descending-ascending) is illustrated: the particle diameter first decreased for five layers from 1000 nm to 240 nm and subsequently became larger and larger for the last four layers. The homogeneity of the top surface is noticeable and might be put down to the more-regular variation of the particle diameters in the descending or ascending parts (the diameter ratios between consecutive layers were always close to 1.25). One should note that breaking of the gold-coated glass substrates to get images of the cross-section of the templates had no influence on their structural integrity, as can be seen in all of the SEM pictures.

Since they were deposited on gold substrates, reflectance spectroscopy was a very-convenient and non-destructive technique to optically characterize the structure of our templates. Measurements were therefore carried out using a microspectrophotometer working at normal incidence in the UV–vis–IR range between 250 and 1650 nm. Similarly to previous observations, regular oscillations known as Fabry–Pérot fringes that testify to the thickness homogeneity could be observed in a certain range of wavelengths (here, between 1200 and 1600 nm), as shown in **Figure 3** for three "Type-II" samples consisting of three consecutive stacks of N layers of 430, 740 and 1000 nm silica particles (with $N = 3$, 5 or 10). While the overall reflectance signal became more and more attenuated when the sample got thicker, the number of fringes resulting from interference phenomena at the air-template and template-substrate interfaces increased as a result of the larger optical pathway. As shown previously,[30,42] the wavelength positions of consecutive reflectance maxima allow the thickness of the samples, θ, to be estimated using Equation 1:

$$m\lambda_1\lambda_{(1+m)} = 2n_e(\lambda_{(1+m)} - \lambda_1)\theta \quad (1)$$

In Equation 1, λ_1 is the wavelength position of the first visible fringe taken into account and n_e is the mean refractive index for a compact arrangement of silica spheres in air, assumed to be close to 1.33. For each sample, θ is therefore equal to the slope of the linear fits plotted in the inset of Figure 3: the calculated values are 5.3, 9.4 and 19.4 µm for the three "Type-II" examples with three consecutive stacks of N layers ($N = 3$, 5 and 10, respectively). These results are in good agreement with the thicknesses inferred either from the SEM observations or from geometrical calculations assuming a face-centred cubic (fcc) packing of spheres in each stack.

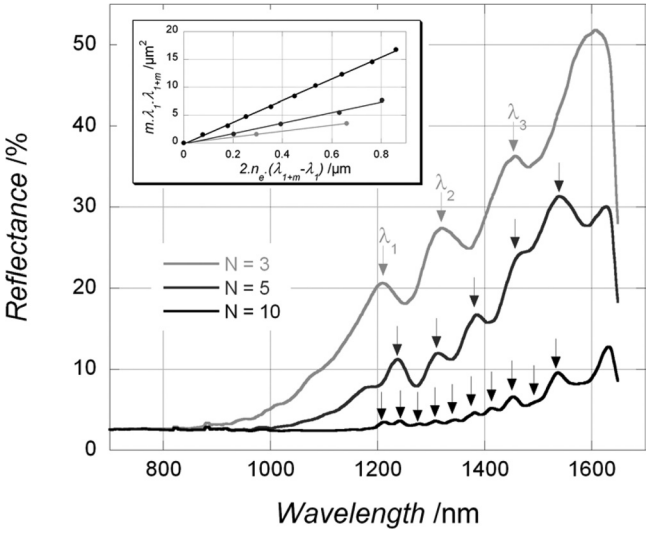

Figure 3. UV–vis–near-IR (NIR) reflectance spectra of three "Type-II" templates consisting of three consecutive stacks of N layers of silica particles with an increasing diameter (430 nm for the first stack, 740 nm for the second and 1000 nm for the third). The arrows indicate the positions of the Fabry–Pérot fringes that were taken into account when calculating the thickness of each sample, equal to the slope of the linear fits shown in the inset.

© 2012 WILEY-VCH Verlag GmbH & Co. KGaA, Weinheim

2.2. Gold Electrodeposition into the Colloidal-Crystal Templates

In a subsequent step, the templates fabricated in Section 2.1 served as working electrodes for the electrodeposition of gold. A commercially available plating solution containing brightener was used for all of the experiments and a constant potential of –660 mV versus Ag/AgCl was applied in order to reduce the gold sulphite ions into metallic gold. In all of the figures presented below, for the sake of clarity, the intensity of the faradaic current signal that was recorded during the electrodeposition process has been divided by the geometrical surface area of the electrode. A typical example of such a chronoamperometric curve, recorded for the "Type-I" sample shown in Figure 2a, is presented in **Figure 4**a.

As observed in previous work dealing with cylindrical substrates,[6] it was particularly easy and straightforward to follow the growth of the metallic deposits in these homogeneous and crack-free colloidal templates thanks to the current-density variations: here, around a mean value of about –0.5 mA cm^{-2}. Indeed, the local extrema of the current density can be attributed to the periodic variation of the electroactive surface area of the growth front during the gold deposition. Since we are dealing with a reduction process, the current density is negative and its absolute value reaches a minimum when the electroactive area is minimal. This occurs when the altitude z of the electrodeposition front (or thickness of the deposit) equals an odd number of half-layers (i.e., when $z = r$, $r + a_0$, $r + 2a_0$, etc., with r being the radius of the particles and a_0 the lattice constant of the pseudo fcc arrangement of particles). The shape of these oscillations depends on the particle diameter, larger ones resulting in a longer oscillation period. From Figure 4a, the mean period in every stack could be estimated as 15 min (first 1000 nm stack), 9 min (intermediate 430 nm stack) and, finally, 20 min (second 1000 nm stack), suggesting a slight decrease of the growth velocity due to an increase of the ohmic losses when the gold-silica composite became thicker.

Another remarkable feature was particularly visible when the electrodeposition occurred in the templates containing large particles. As expected but never observed experimentally by other authors,[43] the interpenetration of two consecutive layers of particles in an fcc arrangement should generate a local extremum for the current density when the electrodeposition front reaches the middle of the junction between two consecutive layers. As shown in the inset in Figure 4a, the first minimum in the current density indeed presented a small local maximum, thus corresponding to a local minimum of the electroactive surface area. This observation is in perfect agreement with the theoretical variation of the available surface area, calculated as a function of the altitude z of the growth front in the same Type-II template (5 layers of 1000 nm, 5 layers of 430 nm, 5 layers of 1000 nm). Assuming the velocity of the electrodeposition process is constant, this z-dependency, plotted in Figure 4b, can be considered as a function of time. Two symmetrical cusps were observed around the extrema for each even number of half-layers ($z = 2r$, $2r + a_0$, etc.) illustrating the anti-monotone surface-area variation in the overlap zone of two consecutive layers.

Three other characteristics emerged from this theoretical calculation based on pure geometric considerations. Firstly, the

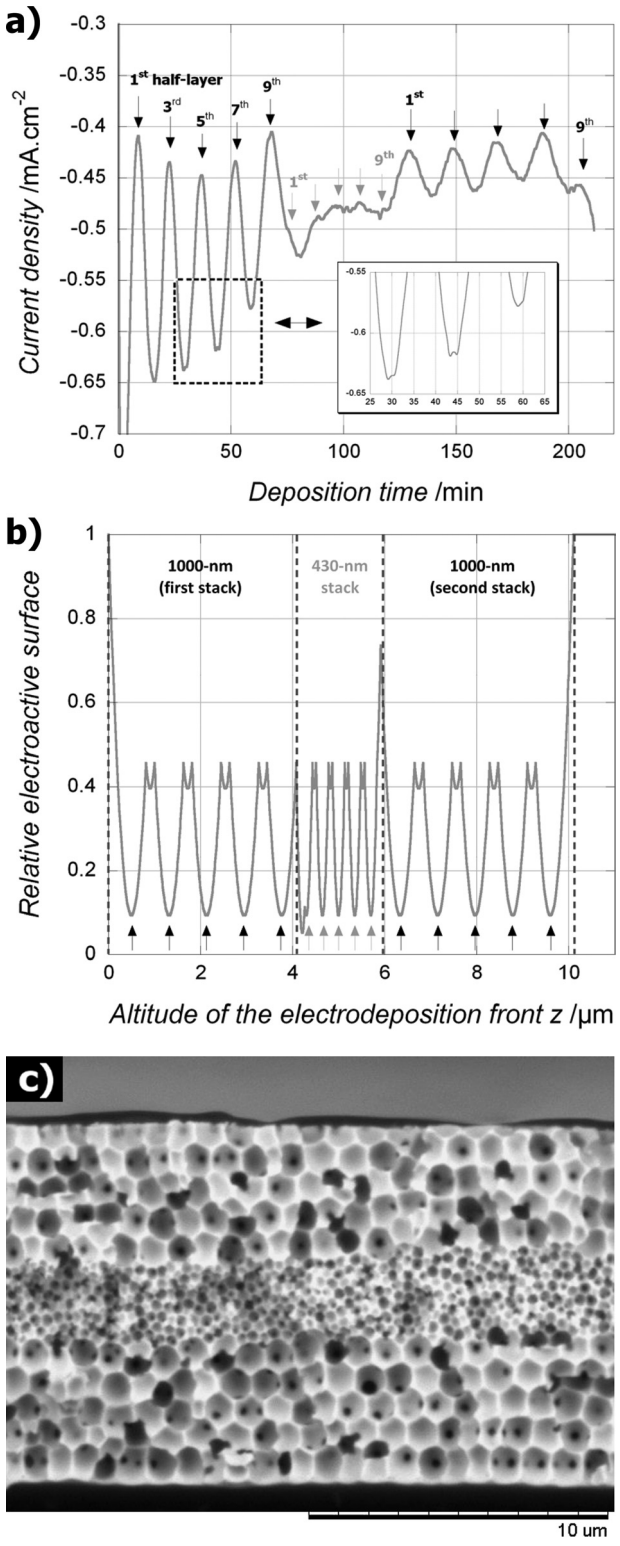

Figure 4. a) Chronoamperometric curve corresponding to the electrodeposition of gold in a Type-I template presenting an artificial planar defect with two 5-layer stacks of 1000 nm particles separated by a 5-layer stack of 430 nm particles. Potential for the deposition: E = –660 mV (versus $E_{Ag/AgCl}$). b) Theoretical calculation of the electroactive area as a function of the position of the progressing electrodeposition front. c) SEM image of the final gold structure after the removal of the template.

© 2012 WILEY-VCH Verlag GmbH & Co. KGaA, Weinheim

absolute minimal area should be equal to 10% of the whole surface for each half-layer thickness, in agreement with the value of 0.9 for the surface compactness – or packing parameter – expected for a hexagonal pavement of disks. It is worth noting that this minimum value is independent of the diameter of the particles. Secondly, the variation of the surface in the overlap between two consecutive stacks around values of z close to 4.2 and 5.9 µm also exhibits local extrema that are not visible experimentally. Finally, when the metallic deposit reaches the top surface of the template, the electrochemically active area increases again, up to a maximum value (i.e., the geometrical surface of the bare substrate). This last feature was, however, not observed in our experiments, since we systematically stopped the electrochemical reaction just before the gold deposit reached the top surface. To be more precise, the electrodeposition was performed until observation of the last maximum, corresponding to the 9th half-layer in Figure 4a. Some other examples are presented in **Figure 5**a, where the gold reduction was carried out in "Type-II" templates consisting of three stacks of particles with an increasing diameter. For the samples with cross-sections presented in Figure 5b and 5c, the process was stopped after the 5th and the 19th half-layers of their respective third stacks, consisting of 3 or 10 layers of 1000 nm silica particles. This was done in order to allow the dissolution of the silica template, requiring diffusion of a dilute solution of hydrofluoric acid from the top surface to the bottom of the electrode, which otherwise would not be possible. After removal of the templates, the final macroporous materials presented interconnected voids and a top surface with a remarkable flatness, illustrating the homogeneity of the electrodeposition process due to both the adequate plating solution and the template quality. This was particularly illustrated by the registered current transients, drawn in Figure 5a, where almost every maximum of the current was resolved (up to 30 for the "Type-II" sample shown in Figure 5c), whereas the best results described in the literature quote the detection of a mere 10 maxima in the current density.[44]

Additional experiments were also carried out under similar conditions using the "Type-III" templates that are shown in Figure 2c and 2d. Again, the variation of the current density versus time had to be correlated to the architecture of the template, the amplitude of the oscillations decreasing slowly during the electrodeposition process, either due to a laterally inhomogeneous growth front of the gold deposit or a slight imperfection in the ordering of the colloidal particles in the template.

A good example for this last-mentioned point is presented in **Figure 6**a with the "ascending-descending" sequence. For the sake of clarity, the structure of the template is recalled at the top of the figure using spheres that are positioned symmetrically around each extremum (corresponding to each half-layer) and whose sizes are exactly proportional to the actual size of the silica particles used experimentally. Indeed, the corresponding chronoamperometric curve is particularly remarkable since the first six current oscillations, related to each of the six monolayers of the "ascending" stack, are clearly visible and their period matches almost perfectly with the size of the particles. However, electrodeposition in the "descending" stack generated less-pronounced oscillations. This result is in good agreement with the SEM image of the obtained inverse material, shown in Figure 6b, where a highly ordered porous structure is observed

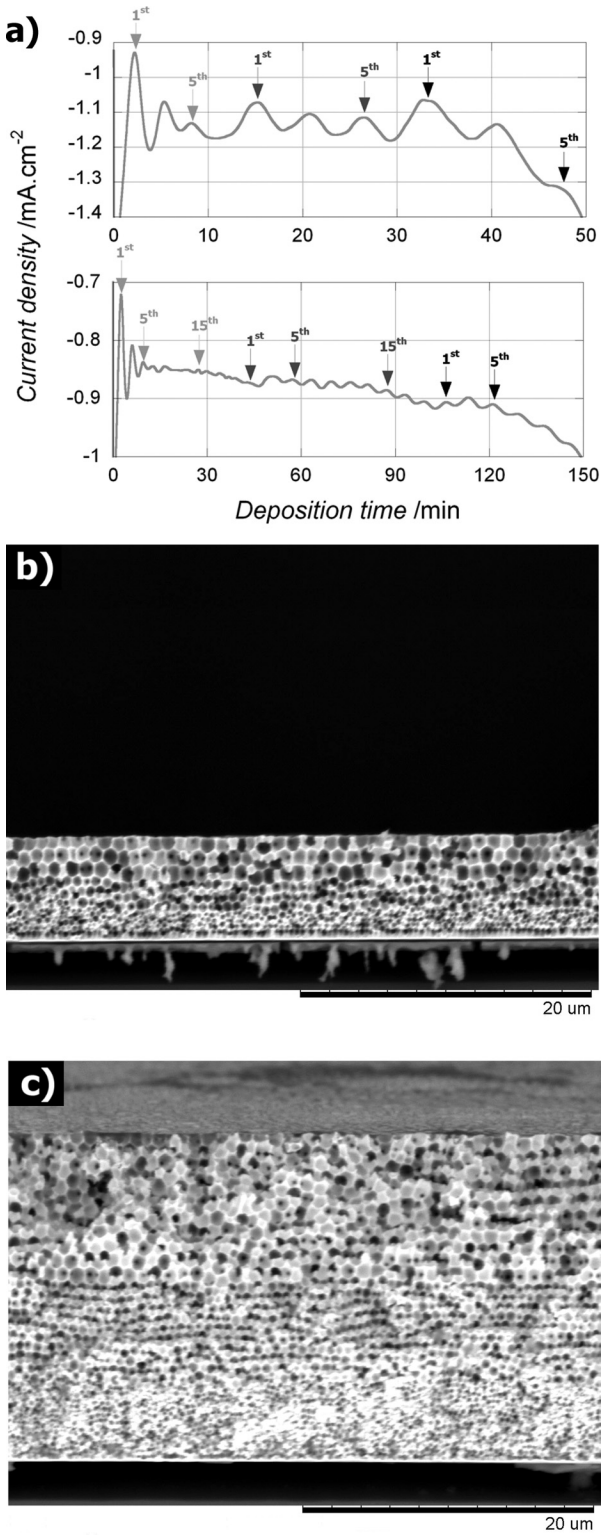

Figure 5. a) Chronoamperometric curves corresponding to the electrodeposition of gold in a "single-gradient" template consisting of three consecutive stacks of N (N = 3 or 10) layers of 430, 740 and 1000 nm particles. Potential for the deposition: E = –660 mV (versus $E_{Ag/AgCl}$). The arrows indicate the maxima corresponding to significant half-layer positions in each stack. b–c) SEM images of the corresponding materials after removal of the template for N = 3 and N = 10, respectively.

© 2012 WILEY-VCH Verlag GmbH & Co. KGaA, Weinheim

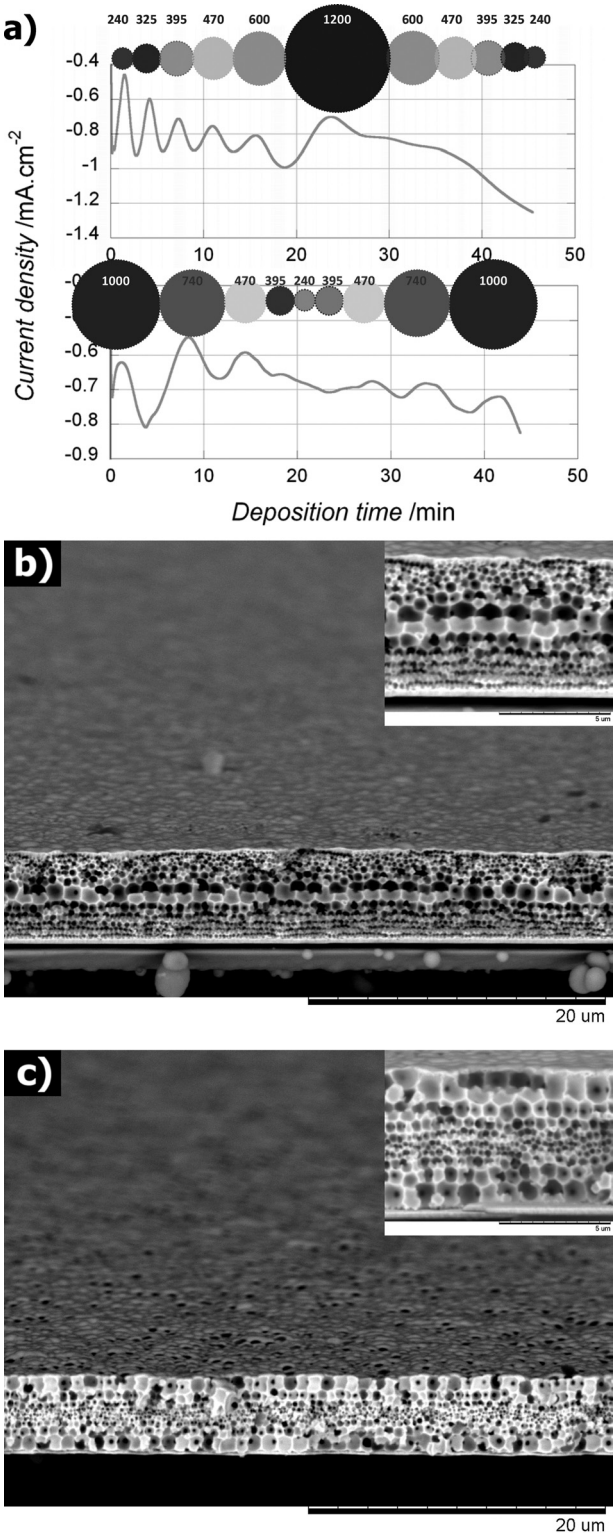

Figure 6. a) Chronoamperometric curves corresponding to the electrodeposition of gold in "Type-III" double-gradient templates with ascending-descending and descending-ascending structures (numbers on spheres indicate the diameter of the particles used in the template). Potential for the deposition: $E = -660$ mV (versus $E_{Ag/AgCl}$). b–c) SEM images of the corresponding gold macroporous replicas after the removal of the inorganic template.

in the lower part of the sample (until the middle layer), whereas the degree of disorder was higher in the upper five layers, this being directly attributable to the stacking irregularities observed in the template (see Figure 2c). On the contrary, electrodeposition in the "descending-ascending" structure, where the variation in the particle size was more progressive between consecutive layers, led to a much-more-symmetrical chronoamperometric profile, the maxima of the current density being still visible in the second "ascending" stack.

2.3. Polypyrrole Electrodeposition into the Colloidal-Crystal Templates

Besides gold, plenty of other metals like zinc, nickel, copper, silver or platinum,[45–49] as well as polymeric materials,[50,51] can be successfully electrodeposited onto a conductive surface using commercially available or homemade plating solutions. To illustrate that our results depended mainly on the quality of the template, the electrodeposition of a conducting polypyrrole film, starting from a freshly prepared pyrrole solution, was carried out at a potential of +600 mV versus $E_{Ag/AgCl}$, following a protocol inspired from the literature.[52]

Figure 7a presents the chronoamperometric curves obtained during electrodeposition within "Type-III" templates that were identical to those used in Figure 6. Since the formation of polypyrrole results from an oxidation process of pyrrole, the faradaic current has a positive sign and, as a consequence, each current-density minimum now corresponds to a minimum of the electroactive surface.

Similar to the results obtained with the gold plating solution, we again observed regular oscillations of the current density, here around a mean value of 0.3 mA cm^{-2}. In the "ascending" stack of the ascending-descending structure, the interdistance between consecutive maxima was again in perfect agreement with the size variation of the particles from consecutive layers. As expected, oscillations were, however, less visible in the "descending stack" and the flatness of the top surface was also less regular compared with the gold homologue, as can be seen in Figure 7b. On the other hand, electrodeposition in the "descending-ascending" structure led to an almost-perfectly symmetrical chronoamperometric curve, indicating both: i) the good symmetry of the template architecture, and ii) a constant rate of reaction, or film-growth velocity, suggesting that the electrochemical oxidation of the pyrrole proceeded homogeneously. Again, the SEM side view, shown in Figure 7c, obtained after dissolution of the silica particles in dilute HF, confirmed this statement.

3. Conclusions

Three-dimensional colloidal templates, uniform in shape and thickness over a large macroscopic scale (several cm^2) were elaborated through the Langmuir–Blodgett technique on planar, conductive substrates using silica particles of various diameters as basic units. Three different kinds of templates with increasing complexity in their architecture were successfully synthesized: templates with a well-defined planar defect involving two

© 2012 WILEY-VCH Verlag GmbH & Co. KGaA, Weinheim

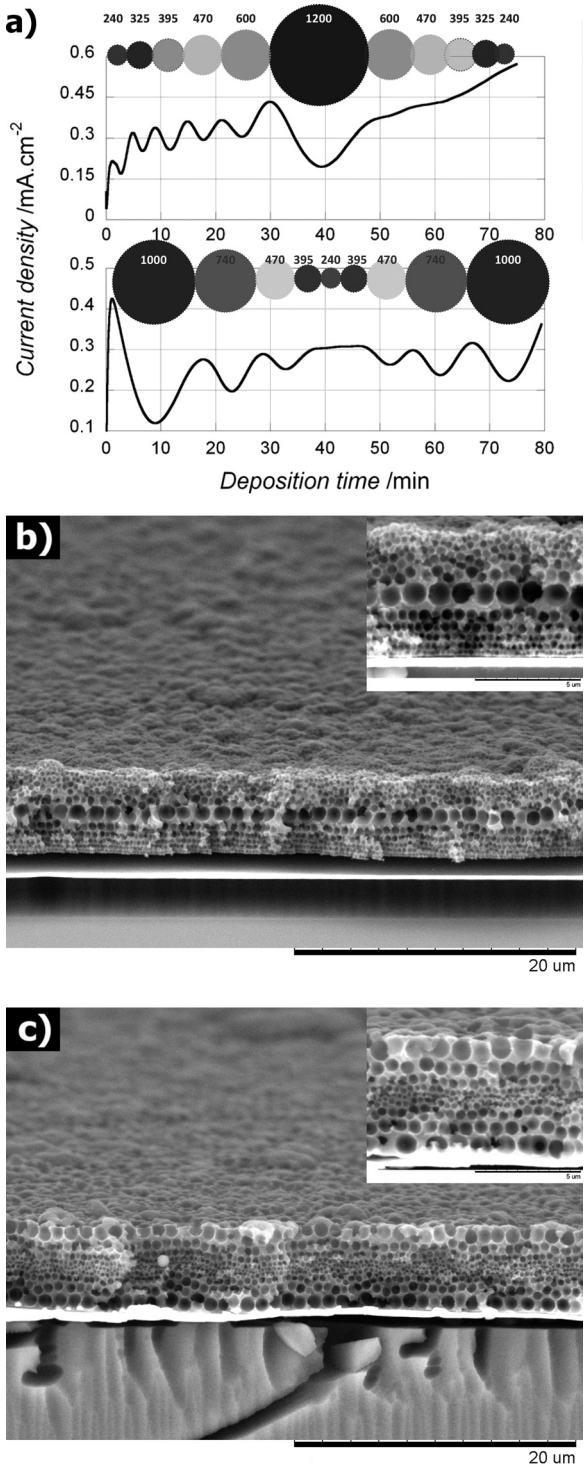

Figure 7. a) Chronoamperometric curves corresponding to the electrodeposition of polypyrrole in "Type-III" double-gradient templates with ascending-descending and descending-ascending structures. Potential for the deposition: E = +600 mV (versus $E_{Ag/AgCl}$). b–c) SEM images of the corresponding materials after the removal of the inorganic template.

different particle diameters (Type-I); templates with a diameter gradient using three stacks of particles with different sizes and thicknesses (Type-II); and, finally, "double-gradient" templates, resulting from a symmetrical stacking of single layers of particles with up to 6 different diameters (Type-III).

Gold or polypyrrole inverse replicas of these superstructures were then generated through electrochemical deposition. Whatever the type of template, the chronoamperometric curves presented similar characteristics, allowing unprecedented control over the electrodeposition process, which could be stopped when necessary. After template dissolution, SEM cross-sectional views of the as-synthesized materials showed highly regular macroporous materials with a uniform thickness and interconnected pores.

4. Experimental Section

Synthesis of the Colloidal Templates: Silica particles of various diameters (240, 325, 395, 430, 470, 600, 740, 1000 and 1200 nm) were synthesized according to batch or semicontinuous procedures inspired from the Stöber sol-gel process based on ammonia-catalyzed hydrolysis and condensation of tetraethoxysilane in a hydroalcoholic medium. Surface modification of these particles with aminopropytriethoxysilane (Aldrich) and the typical washing procedure were then carried out as described previously.[30–32]

Langmuir Film Formation: A dilute suspension of silica particles (approximately 10 mg mL^{-1} of a 80/20 v/v chloroform/ethanol mixture) was spread at the air-water interface of a Langmuir trough filled with double-distilled water. After solvent evaporation, the obtained Langmuir film was compressed stepwise (steps of 1 mN m^{-1}) until the increase of the surface pressure did not modify the area occupied by the particles at the interface. Transfer of a single layer of particles onto a clean glass slide was then carried out to verify the film quality.

Deposition of the LB Films onto Planar Substrates: Gold-coated glass slides were cut into small pieces with a surface between 3 and 4 cm^2 and used as substrates for the LB transfer. After a cautious washing in several solvents (water, acetone and chloroform) to remove all possible contamination from organic molecules, the pieces were kept in an aqueous cysteamine (Fluka) solution overnight to ensure good hydrophilicity of the gold surface through the formation of a self-assembled monolayer. The slides were then used as substrates for the LB deposition, a computer-controlled dipping system allowing immersion and withdrawal through the interface. This procedure was automatically carried out several times, until the desired number of particle layers had been transferred.

Potentiostatic Growth of the Gold Deposit: After the formation of the silica template, the gold-coated slides were used as working electrodes in a typical three-electrode cell with a platinum foil as the counterelectrode and an Ag/AgCl electrode as the reference. A cyanide-free gold-plating bath purchased from Metalor (ECF-63; containing brightener and with a gold concentration of 10 g L^{-1}) was used as received for the metal deposition. A constant potential of –660 mV was applied and the intensity of the faradaic current resulting from the Au-ion reduction was measured using an Autolab PGSTAT 20 potentiostat (EcoChemie) system monitored by a PC running the GPES 4.9 software.

Potentiostatic Growth of the Polypyrrole Deposit: Pyrrole (98%, Sigma–Aldrich) was distilled before use and stored in a closed container in a freezer. A 0.1 M pyrrole aqueous solution of 1 M KCl was sonicated for 5 min in order to allow complete dissolution of the monomer. For the electrodeposition of the polypyrrole, basically the same setup was employed as for the gold deposition with a potential that was kept constant at +600 mV.

Theoretical Calculations: Variations of the electrochemically active surface area of the metallic deposit were calculated as a function of the penetration of the growth front in the template, named z, using Scilab 5.3.0. software.

Spectroscopic Characterization: The UV–vis–NIR spectra were recorded in the 250–1700 nm range using a 20/20 PVTM micro-spectrophotometer

© 2012 WILEY-VCH Verlag GmbH & Co. KGaA, Weinheim

from CRAIC Technologies, working in reflectance mode at normal incidence.

SEM Characterization: The SEM experiments were carried out using a Hitachi TM-1000 table-top microscope.

Acknowledgements

We gratefully acknowledge the Agence Nationale de la Recherche for its financial support of this study through the ANR project HOPE (BLAN07-3-187142), as well as Dr. Nicolas Mano for fruitful discussions.

Received: August 16, 2011
Published online: November 29, 2011

[1] A. Walcarius, *Anal. Bioanal. Chem.* **2010**, *396*, 261.
[2] V. Urbanová, K. Vytras, A. Kuhn, *Electrochem. Commun.* **2010**, *12*, 114.
[3] C. Y. Kuo, S. Y. Lu, S. Chen, M. Bernards, S. Jiang, *Sens. Actuators B: Chem.* **2007**, *124*, 452.
[4] L. Zhao, L. Tong, C. Li, Z. Gu, G. Shi, *J. Mater. Chem.* **2009**, *19*, 1653.
[5] X. Wang, S. M. Husson, X. Qian, S. R. Wickramasinghe, *J. Membr. Sci.* **2010**, *365*, 302.
[6] S. Reculusa, M. Heim, F. Gao, N. Mano, S. Ravaine, A. Kuhn, *Adv. Funct. Mater.* **2011**, *21*, 691.
[7] R. Szamocki, S. Reculusa, S. Ravaine, P. N. Bartlett, A. Kuhn, R. Hempelmann, *Angew. Chem. Int. Ed.* **2006**, *45*, 1317.
[8] L. Deng, F. Wang, H. Chen, L. Shang, L. Wang, T. Wang, S. Dong, *Biosens. Bioelectron.* **2008**, *24*, 329.
[9] Y. Zeng, D. J. Harrison, *Anal. Chem.* **2007**, *79*, 2289.
[10] B. Gates, Y. Yin, Y. Xia, *Chem. Mater.* **1999**, *11*, 2827.
[11] J. H. Holtz, J. S. W. Holtz, C. H. Munro, S. A. Asher, *Anal. Chem.* **1998**, *70*, 780.
[12] P. V. Braun, P. Wiltzius, *Nature* **1999**, *402*, 603.
[13] A. van Blaaderen, R. Ruel, P. Wiltzius, *Nature* **1997**, *385*, 321.
[14] M. Trau, D. A. Saville, I. A. Aksay, *Science* **1996**, *272*, 706.
[15] P. Jiang, M. J. McFarland, *J. Am. Chem. Soc.* **2004**, *126*, 13778.
[16] Z.-Z. Gu, A. Fujishima, O. Sato, *Chem. Mater.* **2002**, *14*, 760.
[17] P. Jiang, J. F. Bertone, K. S. Hwang, V. L. Colvin, *Chem. Mater.* **1999**, *11*, 2132.
[18] S. H. Park, D. Qin, Y. Xia, *Adv. Mater.* **1998**, *10*, 1028.
[19] P. Jiang, G. N. Ostojic, R. Narat, D. M. Mittleman, V. L. Colvin, *Adv. Mater.* **2001**, *13*, 389.
[20] Q. Yan, X. S. Zhao, Z. Zhou, *J. Cryst. Growth* **2006**, *288*, 205.
[21] Q. Yan, A. Chen, S. J. Chua, X. S. Zhao, *Adv. Mater.* **2005**, *17*, 2849.
[22] Y. Jun, C. A. Leatherdale, D. J. Norris, *Adv. Mater.* **2005**, *17*, 1908.
[23] Q. Yan, Z. Zhou, X. S. Zhao, S. J. Chua, *Adv. Mater.* **2005**, *17*, 1917.
[24] F. Fleischhaker, A. C. Arsenault, Z. Wang, V. Kitaev, F. C. Peiris, G. Von Freymann, I. Manners, R. Zentel, G. A. Ozin, *Adv. Mater.* **2005**, *17*, 2455.
[25] N. Tétreault, A. C. Arsenault, A. Mihi, S. Wong, V. Kitaev, I. Manners, H. Miguez, G. A. Ozin, *Adv. Mater.* **2005**, *17*, 1912.
[26] R. Pozas, A. Mihi, M. Ocaña, H. Míguez, *Adv. Mater.* **2006**, *18*, 1183.
[27] J. Li, L. Xue, Z. Wang, Y. Han, *Colloid Polym. Sci.* **2007**, *285*, 1037.
[28] G. Von Freymann, S. John, V. Kitaev, G. A. Ozin, *Adv. Mater.* **2005**, *17*, 1273.
[29] B. van Duffel, R. H. A. Ras, F. C. De Schryver, R. A. Schoonheydt, *J. Mater. Chem.* **2001**, *11*, 3333.
[30] S. Reculusa, S. Ravaine, *Chem. Mater.* **2003**, *15*, 598.
[31] S. Reculusa, P. Massé, S. Ravaine, *J. Colloid Interface Sci.* **2004**, *279*, 471.
[32] S. Reculusa, S. Ravaine, *Appl. Surf. Sci.* **2005**, *246*, 409.
[33] P. Massé, S. Reculusa, K. Clays, S. Ravaine, *Chem. Phys. Lett.* **2006**, *422*, 251.
[34] P. Massé, S. Reculusa, S. Ravaine, *Colloids Surf. A* **2006**, *284–285*, 229.
[35] J. F. Dechézelles, G. Mialon, T. Gacoin, C. Barthou, C. Schwob, A. Maître, R. A. L. Vallée, H. Cramail, S. Ravaine, *Colloids Surf. A* **2011**, *373*, 1.
[36] P. Massé, G. Pouclet, S. Ravaine, *Adv. Mater.* **2008**, *20*, 584.
[37] O. D. Velev, E. W. Kaler, *Adv. Mater.* **2000**, *12*, 531.
[38] O. D. Velev, A. M. Lenhoff, *Curr. Opin. Colloid Interface Sci.* **2000**, *5*, 56.
[39] P. N. Bartlett, J. J. Baumberg, P. R. Birkin, M. A. Ghanem, M. C. Netti, *Chem. Mater.* **2002**, *14*, 2199.
[40] P. N. Bartlett, P. R. Birkin, M. A. Ghanem, *Chem. Commun.* **2000**, 1671.
[41] S. Ben-Ali, D. A. Cook, P. N. Bartlett, A. Kuhn, *J. Electroanal. Chem.* **2005**, *579*, 181.
[42] S. Reculusa, R. Perrier-Cornet, B. Agricole, V. Héroguez, T. Buffeteau, S. Ravaine, *Phys. Chem. Chem. Phys.* **2007**, *9*, 6385.
[43] Y. Hao, F. Q. Zhu, C. L. Chien, P. C. Searson, *J. Electrochem. Soc.* **2007**, *154*, D65.
[44] N. Sapoletova, T. Makarevich, K. Napolskii, E. Mishina, A. Eliseev, A. van Etteger, T. Rasing, G. Tsirlina, *Phys. Chem. Chem. Phys.* **2010**, *12*, 15414.
[45] R. Szamocki, P. Massé, S. Ravaine, V. Ravaine, R. Hempelmann, A. Kuhn, *J. Mater. Chem.* **2009**, *19*, 409.
[46] Y.-J. Huang, C.-H. Lai, P.-W. Wu, L.-Y. Chen, *J. Electrochem. Soc.* **2010**, *157*, P18.
[47] R. Zhu, M. A. McLachlan, D. W. McComb, M. P. Ryan, *ECS Trans.* **2008**, *13*, 1.
[48] P. N. Bartlett, J. J. Baumberg, S. Coyle, M. E. Abdelsalam, *Faraday Discuss.* **2004**, *125*, 117.
[49] M. A. Ghanem, P. N. Bartlett, P. De Groot, A. Zhukov, *Electrochem. Comm.* **2004**, *6*, 447.
[50] P. N. Bartlett, P. R. Birkin, M. A. Ghanem, C.-S. Toh, *J. Mater. Chem.* **2001**, *11*, 849.
[51] L. Santos, P. Martin, J. Ghilane, P.-C. Lacaze, H. Randriamahazaka, L. M. Abrantes, J.-C. Lacroix, *Electrochem. Commun.* **2010**, *12*, 872.
[52] S. Ghosh, G. A. Bowmaker, R. P. Cooney, J. M. Seakins, *Synth. Met.* **1998**, *95*, 63.

© 2012 WILEY-VCH Verlag GmbH & Co. KGaA, Weinheim